The Lever Arm Effects a Mechanical Asymmetry of the Myosin-V-Actin Bond

J. Christof M. Gebhardt,[†] Zeynep Ökten,[‡] and Matthias Rief[§*]
[†]Physik-Department E22, Technische Universität München, Garching, Germany; [‡]Institut für Zellbiologie, Ludwig-Maximilians-Universität, Munich, Germany; and [§]Munich Center for Integrated Protein Science, Munich, Germany

ABSTRACT Myosin-V is a two-headed molecular motor taking multiple ATP-dependent steps toward the plus end (forward) of actin filaments. At high mechanical loads, the motor processively steps toward the minus end (backward) even in the absence of ATP, whereas analogous forward steps cannot be induced. The detailed mechanism underlying this mechanical asymmetry is not known. We investigate the effect of force on individual single headed myosin-V constructs bound to actin in the absence of ATP. If pulled forward, the myosin-V head dissociates at forces twice as high than if pulled backward. Moreover, backward but not forward distances to the unbinding barrier are dependent on the lever arm length. This asymmetry of unbinding force distributions in a single headed myosin forms the basis of the two-headed asymmetry. Under load, the lever arm functions as a true lever in a mechanical sense.

INTRODUCTION

Myosin-V is an actin based two-headed molecular motor that contributes to cargo transport in vivo (1,2). It takes consecutive ~36 nm steps coupled to ATP hydrolysis toward the plus end (forward) of the filament under low force conditions in vitro (3,4). Each step, a power-stroke of its leading lever arm (5–8) is thought to swing the rear head forward, leading to hand-over-hand movement (9). Between steps, the motor mostly dwells on actin in an asymmetric conformation with its rear head in a poststroke state and its leading head in a prestroke state, respectively (10,11).

In the cell, stronger motors like kinesin are found to pull on the same vesicles as myosin-V (12). It is conceivable that myosin-V in vivo encounters resisting (backward) forces exceeding its stall force of ~2 pN (13). It was observed recently that myosin-V forcedly takes consecutive backward steps under such high force conditions in vitro (14). It was suggested that power-stroke reversal is involved in backward stepping, but the detailed mechanism still remains elusive.

The effect of force on the chemical cycle of myosin-V has been investigated recently on single headed constructs (15–17). Here, we study the effect of force on the mechanical stability of the bond between single headed myosin-V molecules and actin in the absence of ATP. We use myosin-V constructs with varying lever arm lengths to clarify any occurrence of lever arm rotation.

MATERIALS AND METHODS

Proteins

Myosin-V constructs

All DNA manipulations were done according to standard procedures and as instructed by manufacturers. The chicken myosin-V DNA was truncated at R904 to create the single-headed myosin-V-6IQ and at R863 to create myosin-V-4IQ constructs, respectively. Proteins were N-terminally Flag-tagged (GDYKDDDDK) to facilitate protein purification and C-terminally yellow fluorescent protein (YFP)-tagged for specific binding to anti-green fluorescent protein (GFP) antibody beads for single molecule assays. For protein expression in S9 cells, the myosin-V DNA and calmodulin DNA (*Drosophila melanogaster*) was cloned into the pFastBac Dual Vector (Invitrogen, Karlsruhe, Germany) using the restriction sites Nhe I/Kpn I for the myosin-V and Not I/Sal I for the calmodulin gene, respectively. Recombinant virus was generated according to manufacturer's instruction.

Proteins were expressed using the Baculovirus Expression System (Invitrogen) in insect cells (*Spodoptera frugiperda* (Sf9)) according to the manufacturer's instructions. The following protocol refers to 200 mL suspension culture at 2×10^6 cells/mL. For protein purification virus-infected insect cells were pelleted by centrifuging for 15 min at 3500 rpm after 48 h incubation at 28°C. Using a glass homogenizer, cells were carefully lysed in lysis buffer (20 mM imidazole, pH 7.5, 200 mM NaCl, 4 mM $MgCl_2$, 0.5 mM EDTA, 1 mM EGTA, 7% sucrose, 5 mM DTT, 2 mM ATP, 0.5% Igepal, Complete protease inhibitor cocktail (Roche, Mannheim, Germany)). Lysed cells were pelleted by centrifugation for 10 min at 30,000 rpm. The supernatant was incubated with 500 μL ANTI-Flag M2 Affinity Agarose gel (Sigma-Aldrich, Munich, Germany) for 2 h. The beads were washed with 3 mL wash buffer (20 mM imidazole, pH 7.5, 150 mM KCl, 5 mM $MgCl_2$, 1 mM EDTA, 1 mM EGTA, 5 mM DTT, 3 mM ATP). The protein was eluted in 200 μL elution buffer (20 mM imidazole, pH 7.5, 150 mM KCl, 5 mM $MgCl_2$, 1 mM EDTA, 1 mM EGTA, 5 mM DTT, 3 mM ATP, 0.2 mg/mL 1× Flag peptide (Sigma-Aldrich)).

Actin

G-actin was isolated from rabbit skeletal muscle as described in Pardee and Spudich (18). Dual-labeled actin was polymerized essentially as described in Herm-Götz et al. (19). In brief, gelsolin was polymerized together with G-actin (covalently labeled with atto-488 in a molar ratio of 1:50) and stabilized with phalloidin. The resulting small gelsolin-capped filaments were used as polymerization seeds and further elongated by polymerization at their minus end with plain G-actin and stabilized with rhodamin-phalloidin.

Experimental setup

Specific binding of proteins

Myosin-V constructs were specifically bound to anti-GFP labeled beads via the C-terminal YFP molecule. Amino-beads (0.5 μm diameter;

Submitted September 24, 2009, and accepted for publication October 15, 2009.

*Correspondence: mrief@ph.tum.de

Editor: Claudia Veigel.

0006-3495/10/01/0277/5 $2.00

doi: 10.1016/j.bpj.2009.10.017

Polysciences, Eppelheim, Germany) were covalently labeled with Protein-G (Sigma-Aldrich) via a glutaraldehyde-coupling kit (Polysciences) and subsequently labeled with anti-GFP-antibody (Sigma-Aldrich) specific against aa 132–144 (conserved in both GFP and YFP). The concentration of motor proteins was adjusted to ensure $<<1$ protein per bead. Control experiments without motor showed no binding to surface or actin.

Dual-labeled actin filaments were bound to a coverslip by NEM-modified myosin-II as described previously (14). Alignment was achieved by slow longitudinal flow.

Trapping assay

The experimental assay buffer contained 25 mM imidazole·HCL, pH 7.4, 25 mM KCl, 1 mM EGTA, 10 mM DTT, and 4 mM $MgCl_2$ as well as an oxygen-scavenging system (6 mg/mL glucose oxidase, 1 mg/mL catalase, and 1% glucose). To achieve single molecule conditions, the storage solution of the motor was diluted by a factor of $(5 - 20) \times 10^5$, yielding a residual concentration of <0.006 μM ATP in the assay buffer. At this ATP concentration a maximum average of 2 ATP molecules per experiment binds to the actin associated motor (ATP binding at 1.6 $\mu M^{-1}s^{-1}$ (20)), resulting in <2.5% of unbinding events caused by ATP binding or with bound ADP. Because actin free ADP release occurs at 1.2 s^{-1} (20), any ADP molecule bound to the motor directly after dilution should be dissociated by the starting time of the experiment ~5 min later.

Optical tweezers apparatus

We used stable optical tweezers with a 1064 nm laser (Spectra Physics, Darmstadt, Germany). The beam passed through a Faraday isolator (Soliton, Gilching, Germany) to prevent back reflection of laser light. The trapping potential was formed by an oil immersion objective (NA 1.45; Olympus, Hamburg, Germany). After collimation with an oil immersion condenser (NA 1.4; Olympus), bead displacements were detected in the back focal plane with a PSD (Silicon Sensors, Berlin, Germany). A DSP board (GBM, Mönchengladbach, Germany) was used for precision steering of a Piezo microscopy table (PI, Karlsruhe, Germany). Calibration of beads was carried out with the protocol introduced by Tolić-Nørrelykke et al. (21) and all relevant corrections to the power spectrum (22). Data were recorded at 5 kHz (NI, Munich, Germany) and further filtered with a 50 ms window before analysis. Fluorescence of the actin filaments was observed in objective type TIRF, with blue (473 nm) and green (532 nm) excitation lasers (Roithner, Vienna, Austria).

Data analysis

Determination of rupture forces

Force versus time traces were recalculated as force versus extension traces and fit by a worm-like chain model (23) to account for nonlinear compliance. The rupture force was defined as the intercept between the worm-like chain curve and a line fitted to the relaxation part of the bead directly after a rupture event.

Rupture force histograms

We used a two-state model to describe myosin-actin bond rupture (24). The two parameters characterizing bond rupture are the unloaded dissociation rate k_0 and the unbinding distance to the unbinding barrier Δx^*. The probability $P(F)$ that rupture occurs at a certain force F is given by

$$P(F) = 1 - \exp\left(- \int_0^F k_0 \exp(F'\Delta x^*/k_B T)/\dot{F}'(F')dF' \right)$$

(k_B, Boltzmann constant; T, absolute temperature) (25). The loading rate $\dot{F}(F)$ is dependent on force due to the nonlinear compliance of the myosin-actin-bead system. It is given as the slope of the force versus time curve immediately before a rupture event. This has to be taken into account when calculating the rupture force probability density $dP(F)/dF$, which can be fitted to the rupture force distributions. Within our least-squares fitting procedure, we therefore calculated an average $P(F)$ considering all measured loading rates $\dot{F}(F)$ before differencing with respect to force. Variable parameters in the fitting procedure were k_0 and Δx^*. Error bars in the rupture force histograms indicate statistical errors with size $\sqrt{n}$ (n, number of data points in a bin) and were included in the fitting routine. Error bars of fitting values combine statistical errors and errors estimated from deviations of the best fit values obtained using different bin sizes.

RESULTS AND DISCUSSION

We used an optical tweezers based single molecule assay to study the effect of force on the stability of the myosin-V-actin bond (Fig. 1, *inset*; see Materials and Methods for details). The myosin-V constructs included a lever arm with six IQ motifs (MV-6IQ) or four IQ motifs (MV-4IQ) respectively. Specific binding to beads was ascertained by a YFP fused to the C terminus of the myosin-V. Actin filaments were marked at the plus end with a second fluorescent color to infer their directionality. Beads sparsely covered with motor were positioned above actin filaments that were fixed to the coverslip and moved with constant velocity in both forward and backward directions. In this way, forward and backward forces could be applied to the lever arm in the absence of ATP.

A typical force versus time trace of the MV-6IQ pulled with a velocity of 87 nm/s is shown in Fig. 1. The force increases on MV-6IQ binding to the actin filament. After dissociation of myosin from actin the bead is rapidly drawn toward the trap center. Clearly, an asymmetry of unbinding forces is seen between the forward (negative forces) and backward (positive forces) direction of load application.

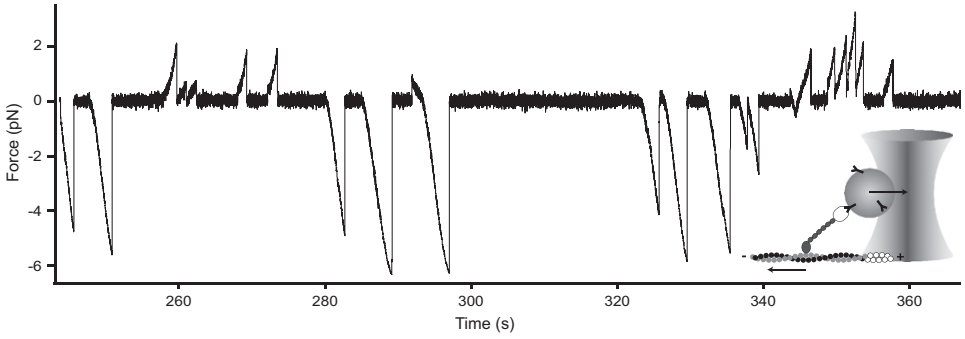

FIGURE 1 Force versus time record of a single headed MV-6IQ molecule at ± 87 nm/s. Positive forces direct toward the minus end of actin and resist the power-stroke of the motor, negative forces direct toward the actin plus end. (*Inset*) Sketch of the experimental setup. Myosin-V constructs were specifically bound to beads via C-terminal YFP molecules. Directionality of the actin filament was inferred from plus end gelsolin marks.

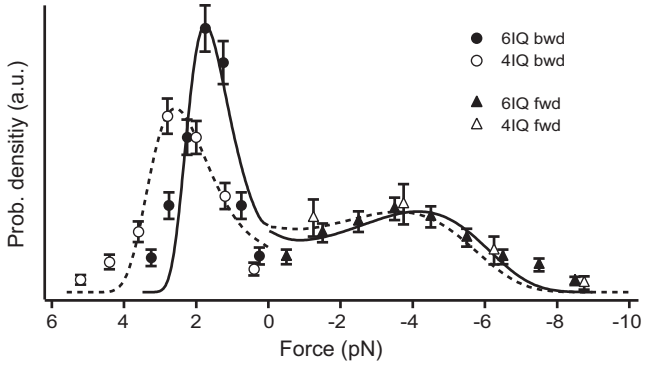

FIGURE 2 Normalized myosin-actin rupture force distributions of MV-6IQ (*solid symbols*) and MV-4IQ (*open symbols*) under backward (*circles*) and forward (*triangles*) directions of load application. Lines are fits to a kinetic Bell model (see Table 1 and Materials and Methods).

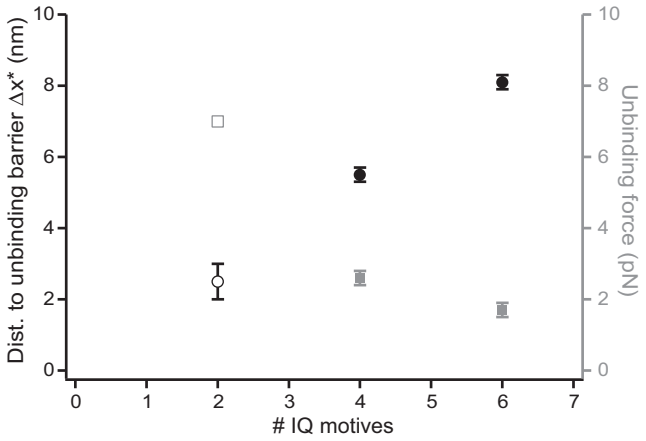

FIGURE 3 Distance to the backward unbinding barrier (*circles*) and unbinding force (*squares*) in the backward direction versus lever arm length given by the number of IQ motifs (~4 nm/IQ (10)). Open symbols refer to data on HMM obtained from Nishizaka et al. (27).

Fig. 2 shows the histogram of unbinding forces of MV-6IQ (*solid symbols*) and MV-4IQ (*open symbols*). In the forward direction (*triangles*), unbinding forces are similar for both constructs and broadly distributed around −4 pN. In contrast, in the backward regime (*circles*), unbinding force distributions are narrow and differ between the two constructs with different lever arm lengths. The distribution of MV-4IQ is broader and shifted to larger forces compared to that of MV-6IQ.

The distributions of unbinding forces were described with a two-state model for bond dissociation (see Materials and Methods) (24). Two parameters characterize a bond in this model, the distance to the unbinding barrier (unbinding distance) Δx^* and the unbinding rate constant in the absence of force, k_0. The most probable dissociation force defines the unbinding force F_{unb}. The results are summarized in Table 1.

Notably, the unbinding distance is unusually large if load is applied in the backward direction (~8 nm for MV-6IQ and ~5.5 nm for MV-4IQ). In contrast, typical values of protein-ligand bond rupture distances are smaller by almost an order of magnitude (26). Therefore, this distance cannot solely be attributed to the rupture of the short range bonds of the myosin-actin binding interface. Instead, a large conformational reorganization of the myosin-actin system is necessary to account for the large unbinding distance.

It is known that the lever arm of myosin-V acts as a lever when performing its power-stroke (6–8). Because the backward unbinding distance corresponds to more than one-third of the power-stroke of the respective construct (6), we anticipate that it is due to lever action of the lever arm. In accordance to this, the backward unbinding distance is proportional to the number of IQ motifs and hence the lever arm length (Fig. 3, *solid circles*). Moreover, the unbinding force decreases with increasing number of IQ motifs.

Previously, Nishizaka et al. (27,28) have studied unbinding forces from actin of single rigor skeletal muscle myosin-II molecules with two IQ motifs at comparable experimental conditions. Interestingly, the fraction of motors bound to actin with one head fits into our observed dependency of unbinding distance and unbinding force on the number of IQ motifs (Fig. 3, *open symbols*).

In contrast to the backward direction, the unbinding barrier distance we find for the forward direction is similar for both constructs (~2.2 nm) and significantly smaller. Lever arm rotation does not seem to dominate the forward unbinding process. This asymmetric behavior can be understood by looking at the asymmetric geometry of rigor myosin-V heads bound to actin: The lever arm draws an angle of ~40° with the actin filament (10). Forward forces will therefore act approximately in the direction of the lever arm, whereas backward forces act on the lever arm with a large angle thus exerting a larger torque.

Two different conformational scenarios are consistent with the lever length dependent rupture forces. In the first model (Fig. 4, *model A*), backward force reverses the myosin head conformation from a poststroke to a prestroke state. As no nucleotides are involved in the experiments, these

TABLE 1 Properties of the myosin-V-actin bond

	Backward force				Forward force			
Construct	F_{unb} (pN)	Δx^* (nm)	$k_{\text{bwd},0}$ (s^{-1})	N	F_{unb} (pN)	Δx^* (nm)	$k_{\text{fwd},0}$ (s^{-1})	N
MV-6IQ	1.7 ± 0.1	8.1 ± 0.2	0.09 ± 0.01	457	4.2 ± 0.2	2.2 ± 0.2	0.12 ± 0.01	288
MV-4IQ	2.6 ± 0.1	5.5 ± 0.2	0.07 ± 0.01	326	3.6 ± 0.3	2.2 ± 0.3	0.13 ± 0.01	46

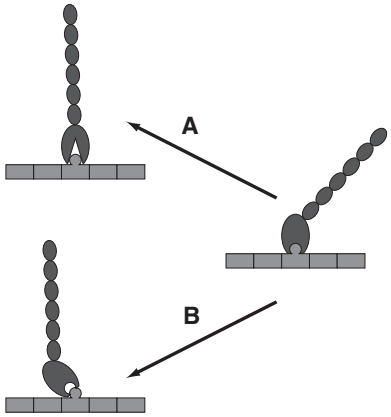

FIGURE 4 Models for the asymmetry of unbinding force distributions. (*A*) Model of power-stroke reversal. Force applied to the end of the lever arm induces conformational changes in the motor domain that decrease the affinity of the head to actin. (*B*) Model of motor domain unrolling. Lever arm and motor domain are rotated simultaneously, thereby amplifying forces and distances needed to break the myosin-actin bond.

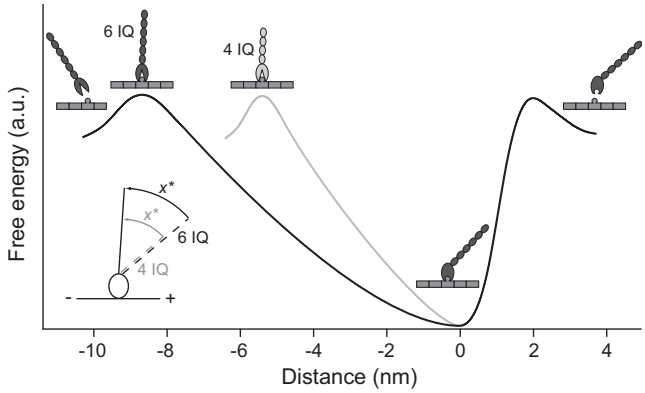

FIGURE 5 Sketch of the asymmetric energy landscape underlying the forced myosin-V-actin bond rupture. The cartoons picture the conformational changes associated with force application. (*Inset*) Sketch depicting the geometry of the myosin-V constructs.

conformations might differ from the structures observed in the presence of nucleotides (29). After reversal of the lever arm, unbinding from actin will occur fast due to the smaller affinity to actin of a myosin head in a prestroke like conformation compared to a head in poststroke conformation (20,30). Note that the unloaded rate constants for myosin unbinding given in Table 1 represent different processes for forward and backward pulling directions. In backward direction, it corresponds to the unloaded rate of power-stroke reversal, in forward direction it represents the rate of unloaded head unbinding. In the second scenario (Fig. 4, *model B*), backward force rotates the lever arm and motor domain simultaneously, peeling the construct off the actin filament. In this case, unbinding distances and forces necessary to break bonds at the myosin-actin interface are amplified by the lever arm. It is important to note that mere bending of the lever arm is not sufficient to explain the large unbinding distances and small backward unbinding forces. Bending of the lever arm would rather add additional compliance to the myosin-actin-bead system but would not affect the unbinding distance. Although we cannot distinguish between both models, model A seems to be more appropriate in the light of experiments on single myosin-V heads in the presence of nucleotide (15–17). The load dependence of nucleotide turnover observed in these experiments is incompatible with a stiff connection between lever arm and motor domain as required by model B.

Our experiments suggest that the mechanical asymmetry in response to high force observed for native myosin-V (14) originates from the asymmetry already present in a single head of myosin-V (Fig. 5). Due to the triangular geometry of two-headed actin-bound myosin-V (10), backward load will predominantly act on the prestroke leading head of the motor, whereas forward load acts on the poststroke rear head. During a forced backward step, the conformation of the head bound to actin is likely reversed due to lever action as observed with the single headed constructs, thereby reducing its affinity to actin and enabling a consecutive backward step. Forward load however acts on a head domain with a lever in poststroke conformation that exhibits larger unbinding forces. Mechanically induced forward steps will therefore be less probable than forcibly induced backward steps.

Directional unbinding forces of the rigor molecule from actin have also been measured in a previous study on the load dependence of the chemical cycle of single headed myosin-V (17). In contrast to our results, Oguchi et al. (17) do not observe the strong asymmetry of unbinding distributions between backward and forward loads as seen in our study. Instead, they find slightly larger unbinding forces for the backward pulling direction than if pulled forward (5.1 and 4.6 pN, respectively). This discrepancy might be due to different attachment chemistries of the motor to the bead and of actin to the glass surface used in both studies.

Recently, an asymmetric unbinding force distribution similar to the distributions shown in Fig. 2 has been measured for skeletal muscle myosin (31). In their work, Lewalle et al. (31) observe lower unbinding forces if the myosin-II head experiences resisting loads compared to forward forces. Although those authors attributed this asymmetry in part to a loading-direction dependent ATP binding rate, we favor the idea that the asymmetric stability of the myosin-II-actin bond is also mediated by lever action. This mechanism may be a common feature of myosins. Moreover, the distance to the unbinding barrier under resisting loads as measured for skeletal muscle by Nishizaka et al. (27) is in accordance with this view (see Fig. 3).

The idea of asymmetry in mechanical stability is emerging also in other molecular systems. An example is mechanical protein stability (32,33). Lever action-induced asymmetry of bond dissociation as in the myosin-actin system is a widely

applicable concept for the achievement of directionality of a molecular bond. A similar lever mechanism might apply also in other protein-protein bonds or in force sensitive conformational changes of molecules (34,35).

We thank S. Köhler for help with covalently labeled actin and M. Reisinger for helpful discussions. Z.Ö. was supported by an EMBO Long-Term fellowship.

This work was supported by Deutsche Forschungsgemeinschaft SFB 486.

REFERENCES

1. Reck-Peterson, S., D. W. Provance, …, J. A. Mercer. 2000. Class V myosins. *Biochim. Biophys. Acta*. 1496:36–51.
2. Wu, X., G. Jung, and J. A. Hammer, 3rd. 2000. Functions of unconventional myosins. *Curr. Opin. Cell Biol.* 12:42–51.
3. Mehta, A. D., R. S. Rock, …, R. E. Cheney. 1999. Myosin-V is a processive actin-based motor. *Nature*. 400:590–593.
4. Rief, M., R. S. Rock, …, J. A. Spudich. 2000. Myosin-V stepping kinetics: a molecular model for processivity. *Proc. Natl. Acad. Sci. USA*. 97:9482–9486.
5. Veigel, C., F. Wang, …, J. E. Molloy. 2002. The gated gait of the processive molecular motor, myosin V. *Nat. Cell Biol.* 4:59–65.
6. Purcell, T. J., C. Morris, …, H. L. Sweeney. 2002. Role of the lever arm in the processive stepping of myosin V. *Proc. Natl. Acad. Sci. USA*. 99:14159–14164.
7. Sakamoto, T., F. Wang, …, J. R. Sellers. 2003. Neck length and processivity of myosin V. *J. Biol. Chem.* 278:29201–29207.
8. Moore, J. R., E. B. Krementsova, …, D. M. Warshaw. 2004. Does the myosin V neck region act as a lever? *J. Muscle Res. Cell Motil.* 25:29–35.
9. Yildiz, A., J. N. Forkey, …, P. R. Selvin. 2003. Myosin V walks hand-over-hand: single fluorophore imaging with 1.5-nm localization. *Science*. 300:2061–2065.
10. Walker, M. L., S. A. Burgess, …, P. J. Knight. 2000. Two-headed binding of a processive myosin to F-actin. *Nature*. 405:804–807.
11. Burgess, S., M. Walker, …, J. Trinick. 2002. The prepower stroke conformation of myosin V. *J. Cell Biol.* 159:983–991.
12. Kural, C., A. S. Serpinskaya, …, P. R. Selvin. 2007. Tracking melanosomes inside a cell to study molecular motors and their interaction. *Proc. Natl. Acad. Sci. USA*. 104:5378–5382.
13. Clemen, A. E., M. Vilfan, …, M. Rief. 2005. Force-dependent stepping kinetics of myosin-V. *Biophys. J.* 88:4402–4410.
14. Gebhardt, J. C. M., A. E. Clemen, …, M. Rief. 2006. Myosin-V is a mechanical ratchet. *Proc. Natl. Acad. Sci. USA*. 103:8680–8685.
15. Purcell, T. J., H. L. Sweeney, and J. A. Spudich. 2005. A force-dependent state controls the coordination of processive myosin V. *Proc. Natl. Acad. Sci. USA*. 102:13873–13878.
16. Veigel, C., S. Schmitz, …, J. R. Sellers. 2005. Load-dependent kinetics of myosin-V can explain its high processivity. *Nat. Cell Biol.* 7:861–869.
17. Oguchi, Y., S. V. Mikhailenko, …, S. Ishiwata. 2008. Load-dependent ADP binding to myosins V and VI: implications for subunit coordination and function. *Proc. Natl. Acad. Sci. USA*. 105:7714–7719.
18. Pardee, J. D., and J. A. Spudich. 1982. Purification of muscle actin. *Methods Cell Biol.* 24:271–289.
19. Herm-Götz, A., S. Weiss, …, D. Soldati. 2002. Toxoplasma Gondii myosin A and its light chain: a fast, single-headed, plus-end-directed motor. *EMBO J.* 21:2149–2158.
20. De La Cruz, E. M., A. L. Wells, …, H. L. Sweeney. 1999. The kinetic mechanism of myosin V. *Proc. Natl. Acad. Sci. USA*. 96:13726–13731.
21. Tolic-Norrelykke, S. F., E. Schaffer, …, H. Flyvbjerg. 2006. Calibration of optical tweezers with positional detection in the back focal plane. *Rev. Sci. Instrum.* 77:103101.
22. Berg-Sorensen, K., and H. Flyvbjerg. 2004. Power spectrum analysis for optical tweezers. *Rev. Sci. Instrum.* 75:594–612.
23. Bustamante, C., J. F. Marko, …, S. Smith. 1994. Entropic elasticity of lambda-phage DNA. *Science*. 265:1599–1600.
24. Friedsam, C., A. K. Wehle, …, H. E. Gaub. 2003. Dynamic single-molecule force spectroscopy: bond rupture analysis with variable spacer length. *J. Phys Condens. Matter*. 15:S1709–S1723.
25. Merkel, R., P. Nassoy, …, E. Evans. 1999. Energy landscapes of receptor-ligand bonds explored with dynamic force spectroscopy. *Nature*. 397:50–53.
26. Neuert, G., C. Albrecht, …, H. E. Gaub. 2006. Dynamic force spectroscopy of the digoxigenin-antibody complex. *FEBS Lett.* 580:505–509.
27. Nishizaka, T., H. Miyata, …, K. Kinosita, Jr. 1995. Unbinding force of a single motor molecule of muscle measured using optical tweezers. *Nature*. 377:251–254.
28. Nishizaka, T., R. Seo, …, S. Ishiwata. 2000. Characterization of single actomyosin rigor bonds: load dependence of lifetime and mechanical properties. *Biophys. J.* 79:962–974.
29. Coureux, P. D., H. L. Sweeney, and A. Houdusse. 2004. Three myosin V structures delineate essential features of chemo-mechanical transduction. *EMBO J.* 23:4527–4537.
30. Rosenfeld, S. S., and H. L. Sweeney. 2004. A model of myosin V processivity. *J. Biol. Chem.* 279:40100–40111.
31. Lewalle, A., W. Steffen, …, J. Sleep. 2008. Single-molecule measurement of the stiffness of the rigor myosin head. *Biophys. J.* 94: 2160–2169.
32. Dietz, H., F. Berkemeier, …, M. Rief. 2006. Anisotropic deformation response of single protein molecules. *Proc. Natl. Acad. Sci. USA*. 103:12724–12728.
33. Bertz, M., M. Wilmanns, and M. Rief. 2009. The titin-telethonin complex is a directed, superstable molecular bond in the muscle Z-disk. *Proc. Natl. Acad. Sci. USA*. 106:13307–13310.
34. Puchner, E. M., A. Alexandrovich, …, M. Gautel. 2008. Mechanoenzymatics of titin kinase. *Proc. Natl. Acad. Sci. USA*. 105:13385–13390.
35. Zhang, X., K. Halvorsen, …, T. A. Springer. 2009. Mechanoenzymatic cleavage of the ultralarge vascular protein von Willebrand factor. *Science*. 324:1330–1334.